Electronic Supplementary Material (ESI) for Materials Advances.

Supporting Information

A study on the effect of phase conversion of tungsten nanostructures on their electrochemical energy storage performance

Visakh V. Mohan[1], P. M. Anjana[1], and R. B. Rakhi[2, 3, *]

[1]*Department of Physics University of Kerala Kariavattom, Thiruvananthapuram, Kerala 695581, India*

[2]*Material Sciences and Technology Division, CSIR- National Institute of Interdisciplinary Science and Technology (CSIR-NIIST), TVM, Kerala, India, 695019*

[3]*Academy of Scientific and Innovative Research (AcSIR), Ghaziabad 201002, India*

**Author for correspondence.*

R. B. Rakhi: rakhiraghavanbaby@niist.res.in; Mobile: +91 9497113659

1. Characterization

The crystallite size of WO_3, $WO_{3-X,}$ and WS_2 electrode materials have been calculated from Debye-Scherrer equation given below,

$$D = \frac{K\lambda}{\beta \cos\theta} \qquad (1)$$

Where D= crystallite Size, K= Debye-Scherrer constant, λ = wavelength of X-ray,

θ = Bragg's angle in radians, and β = the full width at half maximum of the peak in radians.

The crystallite size of WO_3, $WO_{3-X,}$ and WS_2 samples were calculated by using equation 1**.** For WO_3 it's around 57 nm, 29 nm for $WS_{3-X,}$ and 14 nm for $WS_{2.}$ Peak broadening has been observed from the XRD spectra as moving toward the sample WS_2 from WO_3. This is due to the change in crystallite size. Also a shift in XRD pattern for WS_2 sample has been observed, this might be due to the instrumental error.

The optical properties of WO_3, $WS_{3-X,}$ and WS_2 were analysed by UV–visible spectroscopy technique. The optical band gap of each samples were calculated by diffuse reflection spectra (DRS) method with the help Kubelka–Munk equation.

$$F(R) = \frac{(1-R)^2}{2R} \qquad (2)$$

In the equation (2) "*R*" represents the reflectance.

The optical bandgap of the samples were calculated by plotting $[F(R)hv]^n$ vs *hv* graph. Here, '*hv'* is the photon energy and '*n*' is an index which denote the direct or indirect band transitions of the samples **[1]**. For direct band transition value of *n* is 2. In the case of indirect band transition, *n* is ½. In the case of the WO_3 and WO_{3-X} samples the transition is indirect, hence, *n* value is 1/2. Whereas the WS_2 sample possess a direct transition. Hence, *n* value is 2 [1]. The optical bandgap values of the samples were calculated and shown in **Figure S1**. The direct bandgap calculated for the WS_2 sample is 1.7 eV **(figure S1a)**. The optical bandgap of the WO_3 sample is 2.5 eV **(figure S1c)** and that of the WO_{3-X} **(figure S1b)** sample is 2.2 eV.

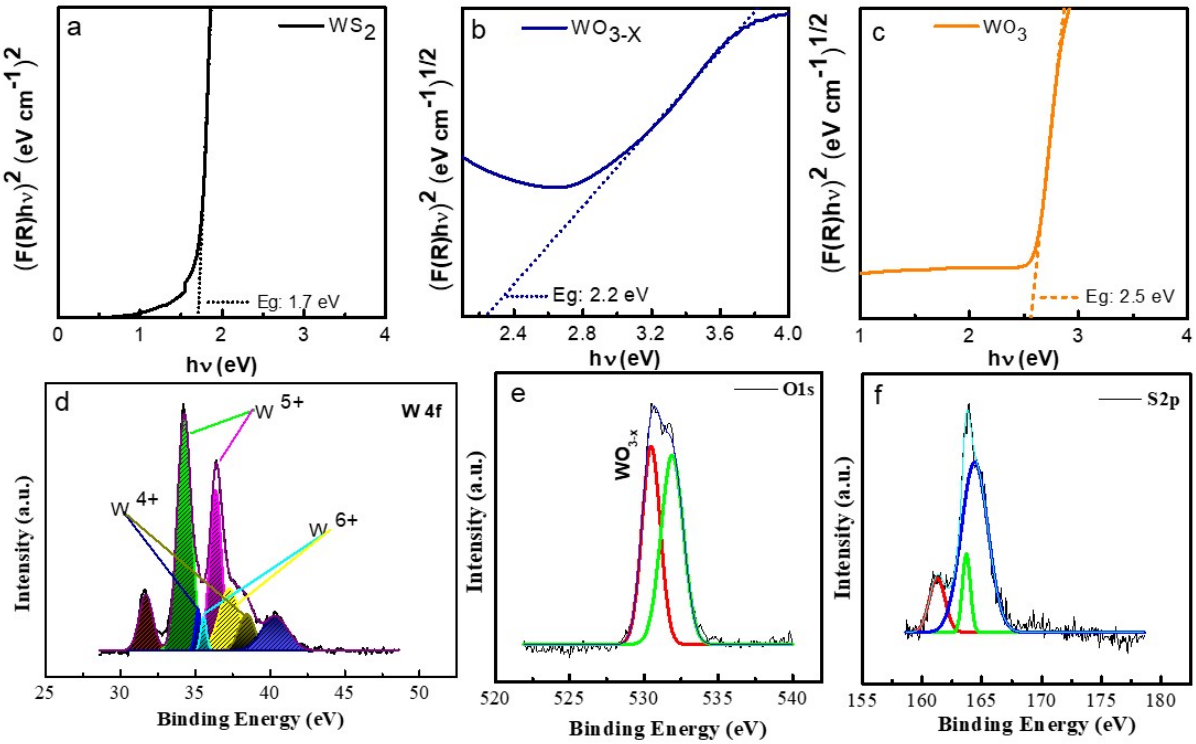

Figure S1: bandgap determation of (a)WO_3 (b)WO_{3-X} (c)WS_2 and XPS analysis d) W4f level e) O1S f) S2p of WO_{3-X} sample

XPS is a quantitative technique used for elemental composition analysis and to determine the chemical states of a system. **Figure S1d** shows the W 4f core-level XPS spectrum of the WO_{3-X} sample. Three doublets are found related to the different oxidation states of 'W'. The minor peaks close to 37.4 eV (W $4f_{5/2}$) and 35.5 eV (W $4f_{7/2}$) correspond to the W atoms having a 6^+ oxidation state, which is due to the presence of WO_3 **[2]**. The two major peaks at 34.3 eV and 36.3 eV are obtained from the emission of $4f_{5/2}$ and W $4f_{7/2}$ core levels, respectively showing the existence of a 5^+ oxidation state **[2]**. It could be noted that two oxidation states of W exist in the sample. This might be due to the oxygen-deficiency and presence of oxygen deficient compound $WO_{2.72}$ (WO_{3-X}) **[2]**. The binding energies at 35.2 and 38.4 eV resulted from the emission of $W4f_{5/2}$ and $W4f_{3/2,}$ which ensure the presence of a 4+ oxidation state of W **due to the** existence of WS_2 in the sample **[3]**. The peak corresponds to 31.7 eV, suggests the presence of 1T-WS_2 in the sample **[4]**.

The XPS spectra of WO_{3-X} for S2p scans are depicted in **figure S1f.** It could be noted that for $WS_{2,}$ energy peaks were found at 163.4 eV and 164.5 eV, which indicate $S2p_{3/2}$ and $S2p_{1/2}$ emissions **[3]**. The peak corresponds to 161.3 eV also ensures the presence of WS_2 in the sample **[5]**. The XPS spectra of the WO_{3-x} sample for the O1s scan is depicted in **figure S1e**.

Here the dominant peak at binding energy 530.5 eV suggests the existence of an oxygen bond with W in $WO_{2.72}$ **[2, 6]**. The second peak at 532 might be due to adsorbed oxygen. Hence there are mainly three states of W found in the WO_{3-X} sample +6, +5, and +4, confirming the presence of both $WO_{2.72}$ and WS_2 **[2-6]**.

2. Fabrication of WO_3, WO_{3-X}, and WS_2 electrodes based symmetric supercapacitors and the evaluation of their electrochemical performance

The cyclic voltammetry (CV)measurements of the symmetric supercapacitors based on WO_3, WO_{3-X}, and WS_2 electrodes were investigated between the potential range 0 to 0.8 V by varying the scan rates from 5 to 200 mV s^{-1}. The quasi rectangular shapes of the CV curves of all three devices indicate that the charge storage mechanism involved is a combination of both double layer and pseudocapacitive behavior **[7,8]**. The Galvanostatic charge–discharge measurements of the symmetric supercapacitors were conducted between the potential ranges 0 to 0.8 V at different current density values from 1 to 5 A g^{-1}.

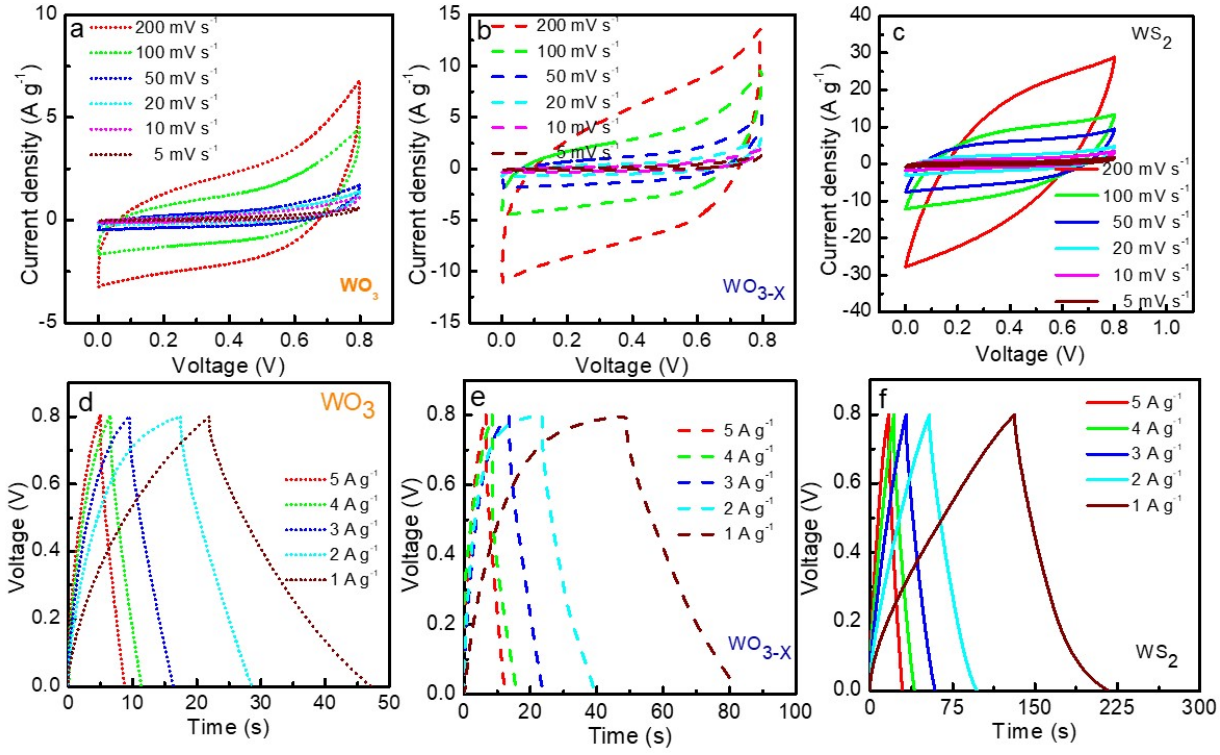

Figure S2. CV curves of (a) WO_3, (b) WO_{3-x}, (c)WS_2 and GCD curves of (d)WO_3, (e) WO_{3-x} (f)WS_2

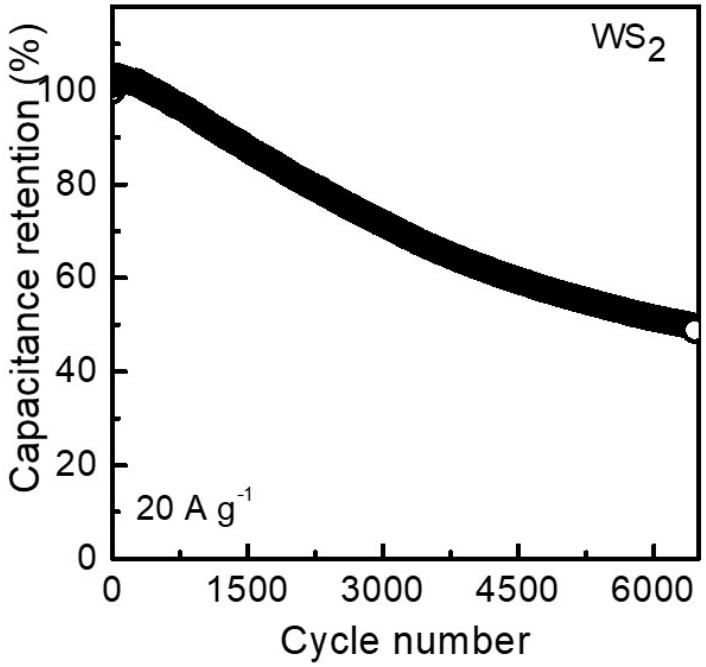

Figure S3: Capacitance retention of WS_2 over 6500 cycles at high current density of 20 A g^{-1}

EIS spectra were fitted using ZSimpWIN3.21 software. **Figure S4a, S4b, and S4c** show the fitted EIS plots of WO_3, $WO_{3-X,}$ and $WS_{2,}$ respectively, and their corresponding equivalent circuits used for fitting are also shown in the figure. Two capacitance and resistance combinations are found. The 1st portion (C_{dl}, R_{ct}) indicates the double-layer formation, and the other portion (C_{dif}, R) indicates the diffusion region. The last portion (W) indicates the Warburg diffusion. The x-intercept in the EIS plot indicates the electrolyte resistance or solution resistance (Rs) which is identified as 1.3 Ω, 1.7 Ω, and 0.8 Ω for WO_3, $WO_{3-X,}$ and $WS_{2,}$ respectively. The straight line in the low-frequency portion makes the angle with the x-axis less than 45° and close to y-axis ensure the capacitive behaviour of the material than the resistive. The diameter of the semicircle region in the EIS represents the charge transfer resistance (R_{ct}) of the electrode material. Symmetric supercapacitors based on WO_3, $WO_{3-X,}$ and WS_2 materials exhibit R_{ct} values of 8.9, 7.6, and 5.8 Ω, respectively. With the lowest R_{ct} value, the WS_2 electrode offers better conductivity and excellent specific capacitance.

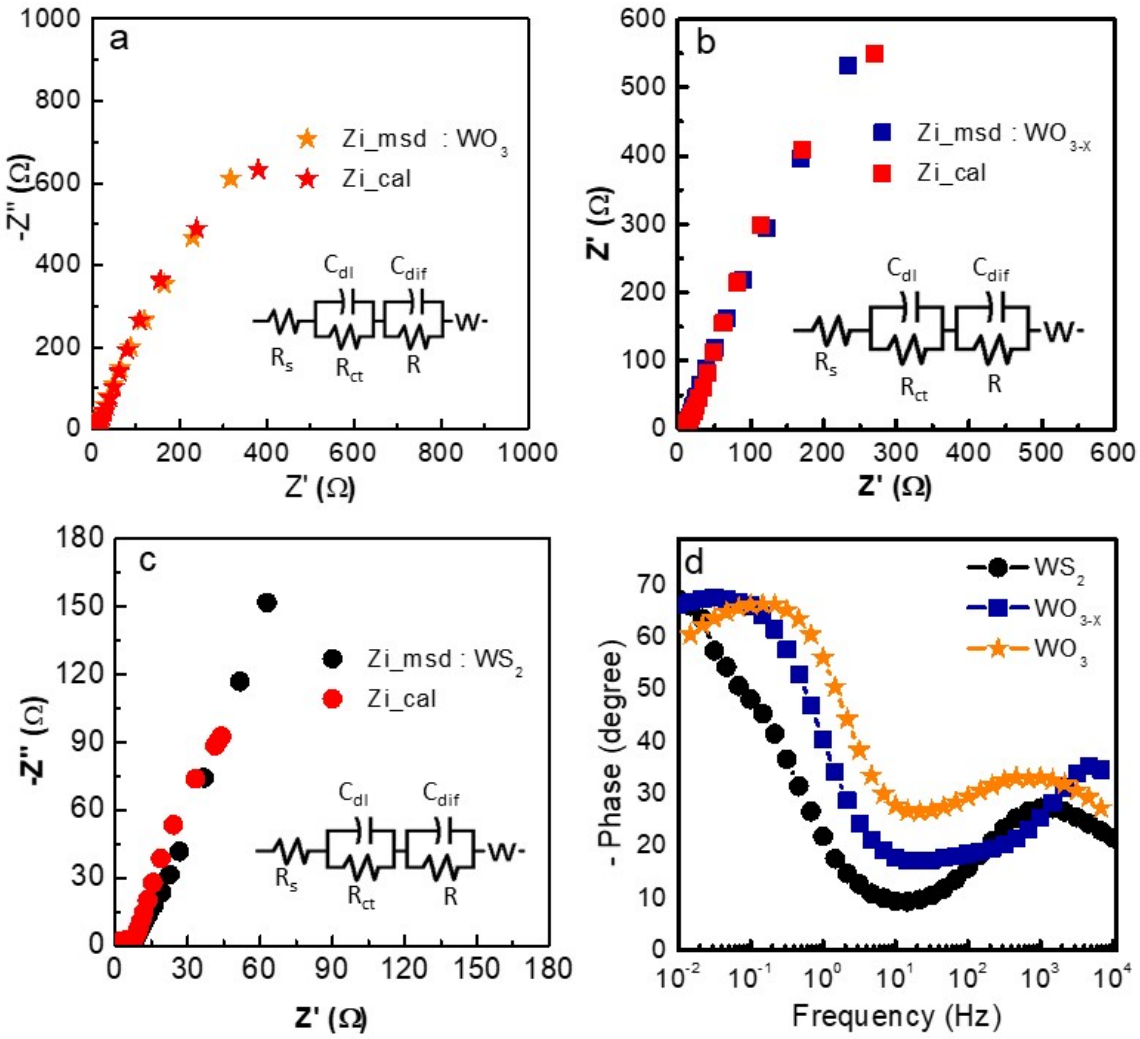

Figure S4: Nyquist plots of **a) WO_3 b) WO_{3-x} c) WS_2. d) Bode plot**

The capacitive properties of WO_3, $WO_{3-X,}$ and WS_2 electrodes were further evaluated from the bode phase angle plots. The bode plot represents the phase of a device as a function of frequency as shown in **Figure S4d**. In the case of an ideal capacitor, the Bode plots represent a 90° phase angle shift in the low-frequency region [14-15]. In the present study, the symmetric supercapacitor based on WO_3 electrodes shows a phase angle closer to 60° in the low-frequency region. In the case of WO_{3-X} electrodes, it is nearly 66°. For WS_2, the phase angle changes to 70◦, indicating an increment in the capacitive contribution as moving from WO_3 to WS_2. The phase angles 60°, 66°, and 70° for WO_3, $W_{3-X,}$ and $WS_{2,}$ respectively, confirm the existence of pseudocapacitive properties [14-15]. The deviation from the ideal capacitive behavior can be related to faradaic charge transfer. [16-18].

The approximate contribution of charge storage kinetics of WO_3, $WO_{3-x,}$ and WS_2 electrode materials can be analysed using the following equation.

$$i = a\, v^b \tag{3}$$

Where (i) is the peak current (v) is the scan rate of the CV loop, 'a' and 'b' are variable parameters. The 'b' value can be calculated by the fitted slopes of log(i) and log(v). The WO_{3-x} and WS_2 electrode materials have 'b' value close to 1 that is b=0.9 and that of WO_3 is b equal to 0.7. Hence the double layer and pseudocapacitive behaviour of electrode materials were found **[9, 10]** (**Figure S5 a**).

The percentage of contribution of charge storage can also be calculated from Trasatti's analysis method **[11-13]**.

$$C_{SP} = \frac{A}{f \times V \times m} F\, g^{-1} \tag{4}$$

$$C = constant * v^{-0.5} + C_{capacitive} \tag{5}$$

$$C^{-1} = constant *\ v^{0.5} +\ C_T^{-1} \tag{6}$$

$$C_T = C_{diffusion} +\ C_{capacitive} \tag{7}$$

Here, A stands for the integral area of current and potential charge obtained from CV curve, the 'm' (mg) in the equation denotes the mass loading of the active material on each electrode, and 'f' (mv s^{-1}) stands for the scan rate. Using Trasatti's analysis method C vs ($1/V^{-1/2}$) and ($1/C$) Vs ($V^{-1/2}$) were plotted for WO_3, $WO_{3-X,}$ and WS_2 based devices and the results are shown in **Figure S5b and c [19].** The percentage of charge storage mechanism for each electrode material is shown in **Figure S5d.**

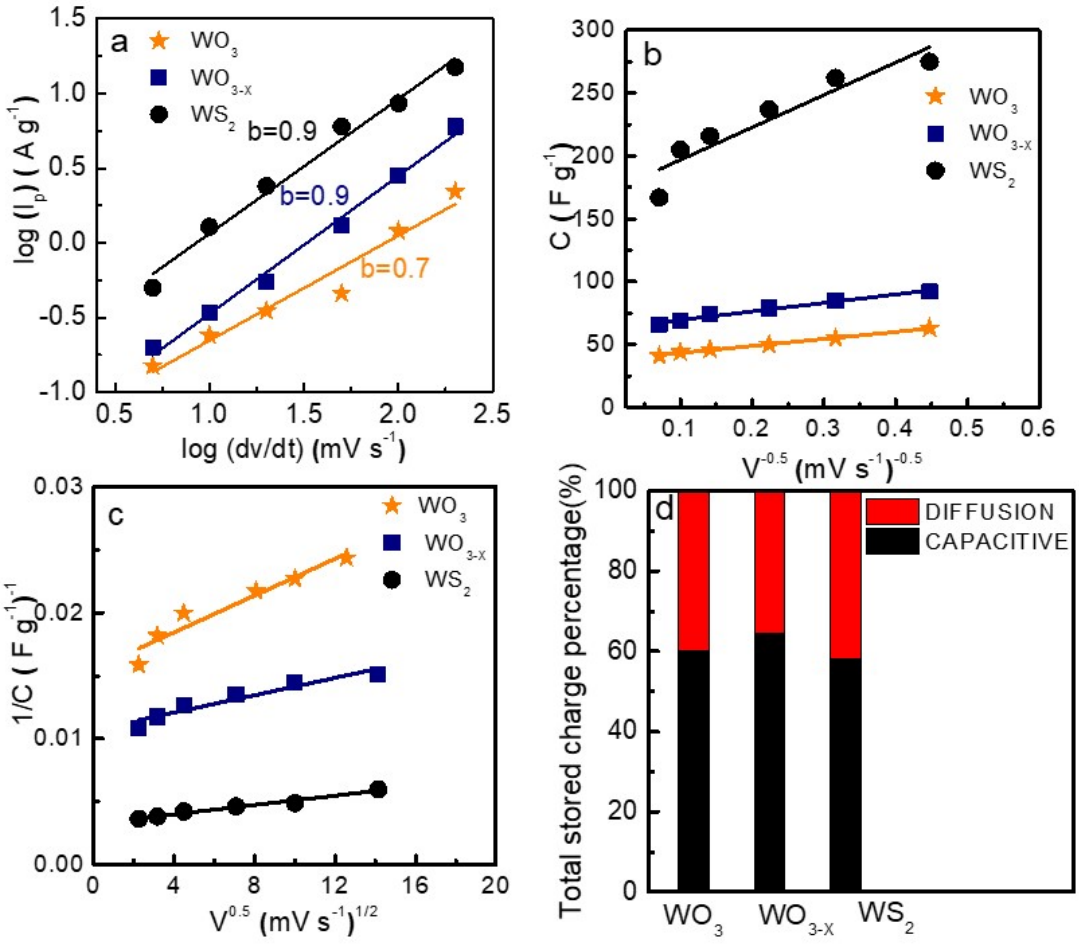

Figure S5. (a) log(ip) Vs log(dv/dt) plot (b) Linear fit of gravimetric specific capacitance (C) vs. reciprocal of square root of scan rate ($v^{-0.5}$), (c) Linear fit of reciprocal of specific capacitance (C^{-1}) vs. square root of scan rate ($v^{0.5}$), (d) percentage of capacitance contribution evaluated for WO_3, WO_{3-X} and WS_2 electrodes based on Trasatti analysis

References

[1] P.J. Boruah, R.R. Khanikar, H. Bailung, Synthesis and Characterization of Oxygen Vacancy Induced Narrow Bandgap Tungsten Oxide (WO3−x) Nanoparticles by Plasma Discharge in Liquid and Its Photocatalytic Activity, Plasma Chem. Plasma Process. 40 (2020) 1019–1036. https://doi.org/10.1007/s11090-020-10073-3.

[2] C. Guo, S. Yin, M. Yan, M. Kobayashi, M. Kakihana, T. Sato, Morphology-controlled synthesis of W 18O 49 nanostructures and their near-infrared absorption properties, Inorg. Chem. 51 (2012) 4763–4771. https://doi.org/10.1021/ic300049j.

[3] M. Habib, A. Khalil, Z. Muhammad, R. Khan, C. Wang, Z. ur Rehman, H.T. Masood, W. Xu, H. Liu, W. Gan, C. Wu, H. Chen, L. Song, WX2(X=S, Se) Single Crystals: A Highly Stable Material for Supercapacitor Applications, Electrochim. Acta. 258 (2017) 71–79. https://doi.org/10.1016/j.electacta.2017.10.083.

[4] D. Escalera-López, R. Griffin, M. Isaacs, K. Wilson, R.E. Palmer, N. V. Rees, Electrochemical sulfidation of WS2 nanoarrays: Strong dependence of hydrogen evolution activity on transition metal sulfide surface composition, Electrochem. Commun. 81 (2017) 106–111. https://doi.org/10.1016/j.elecom.2017.06.016.

[5] F. Perrozzi, S.M. Emamjomeh, V. Paolucci, G. Taglieri, L. Ottaviano, C. Cantalini, Thermal stability of WS2 flakes and gas sensing properties of WS2/WO3 composite to H2, NH3 and NO2, Sensors Actuators, B Chem. 243 (2017) 812–822. https://doi.org/10.1016/j.snb.2016.12.069.

[6] J. Song, Z.F. Huang, L. Pan, J.J. Zou, X. Zhang, L. Wang, Oxygen-Deficient Tungsten Oxide as Versatile and Efficient Hydrogenation Catalyst, ACS Catal. 5 (2015) 6594–6599. https://doi.org/10.1021/acscatal.5b01522.

[7] V. V Mohan, P.M. Anjana, R.B. Rakhi, Materials Today : Proceedings One pot synthesis of tungsten oxide nanomaterial and application in the field of flexible symmetric supercapacitor energy storage device, Mater. Today Proc. (2022). https://doi.org/10.1016/j.matpr.2022.04.046

[8] V. V. Mohan, M. Manuraj, P.M. Anjana, R.B. Rakhi, WS2 Nanoflowers as Efficient Electrode Materials for Supercapacitors, Energy Technol. 10 (2022) 1–7. https://doi.org/10.1002/ente.202100976.

[9] L. Chen, Z. Yang, J. Wu, H. Chen, J. Meng, Energy storage performance and mechanism of the novel copper pyrovanadate Cu3V2O7(OH)2·2H2O cathode for aqueous zinc ion batteries, Electrochim. Acta. 330 (2020) 135347. https://doi.org/10.1016/j.electacta.2019.135347.

[10] Y. Jiang, J. Liu, Definitions of Pseudocapacitive Materials: A Brief Review, Energy Environ. Mater. 2 (2019) 30–37. https://doi.org/10.1002/eem2.12028.

[11] M.R. Thalji, G.A.M. Ali, H. Algarni, K.F. Chong, Al3+ ion intercalation pseudocapacitance study of W18O49 nanostructure, J. Power Sources. 438 (2019) 227028. https://doi.org/10.1016/j.jpowsour.2019.227028.

[12] R. Rajalakshmi, K.P. Remya, C. Viswanathan, N. Ponpandian, Enhanced electrochemical activities of morphologically tuned MnFe2O4nanoneedles and nanoparticles integrated on reduced graphene oxide for highly efficient supercapacitor electrodes, Nanoscale Adv. 3 (2021) 2887–2901. https://doi.org/10.1039/d1na00144b.

[13] Z.H. Huang, T.Y. Liu, Y. Song, Y. Li, X.X. Liu, Balancing the electrical double layer capacitance and pseudocapacitance of hetero-atom doped carbon, Nanoscale. 9 (2017) 13119–13127. https://doi.org/10.1039/c7nr04234e.

[14] J. Shin, Y. Choi, H. Park, Remote Plasma-Induced Synthesis of Self-Assembled MoS 2 / Carbon Nanowall Nanocomposites and Their Application as High-Performance Active Materials for Supercapacitors, (2022).

[15] P. Pazhamalai, K. Krishnamoorthy, S. Manoharan, S.J. Kim, High energy symmetric supercapacitor based on mechanically delaminated few-layered MoS2 sheets in organic electrolyte, J. Alloys Compd. 771 (2019) 803–809. https://doi.org/10.1016/j.jallcom.2018.08.203.

[16] L. Xuan, L. Chen, Q. Yang, W. Chen, X. Hou, Y. Jiang, Q. Zhang, Y. Yuan, Engineering 2D multi-layer graphene-like Co3O4 thin sheets with vertically aligned nanosheets as basic building units for advanced pseudocapacitor materials, J. Mater. Chem. A. 3 (2015) 17525–17533. https://doi.org/10.1039/C5TA05305F.

[17] Yuqian Jiang, Lingyun Chen, Haiqin Zhang, Qing Zhang, Weifan Chen, Jikui Zhu, Dianmei Song, Two-dimensional Co3O4 thin sheets assembled by 3D interconnected nanoflake array framework structures with enhanced supercapacitor performance derived from coordination complexes, Chemical Engineering Journal,292,(2016), 1-12. https://doi.org/10.1016/j.cej.2016.02.009.

[18] Jikui Zhu, Dianmei Song, Tao Pu, Jie Li, Biao Huang, Wensong Wang, Chenglan Zhao, Li Xie, Lingyun Chen, Two-dimensional porous ZnCo2O4 thin sheets assembled by 3D nanoflake array with enhanced performance for aqueous asymmetric supercapacitor, Chemical Engineering Journal, 336 (2018) 679-689. https://doi.org/10.1016/j.cej.2017.12.035

[19] M. Manuraj, V V. Mohan, S. Assa Aravindh, S.R. Sarath Kumar, K.N. Narayanan Unni, R.B. R, Can mixed anion transition metal dichalcogenide electrodes enhance the performance of electrochemical energy storage devices? The case of MoS2xSe2(1-x), Chemical Engineering Journal,443,(2022),136451. https://doi.org/10.1016/j.jpowsour.2021.230747.